UC Berkeley
SEMM Reports Series

Title

An Analysis of Strong Discontinuities in Multiplicative Finite Strain Plasticity and Their Relation with the Numerical Simulation of Strain Localization in Solids

Permalink

https://escholarship.org/uc/item/805979b5

Authors

Armero, Francisco

Garikipati, Krishna

Publication Date

1995-09-01

REPORT NO.

UCB/SEMM-95/09

STRUCTURAL ENGINEERING
MECHANICS AND MATERIALS

AN ANALYSIS OF STRONG DISCONTINUITIES IN MULTIPLICATIVE FINITE STRAIN PLASTICITY AND THEIR RELATION WITH THE NUMERICAL SIMULATION OF STRAIN LOCALIZATION IN SOLIDS

BY

FRANCISCO ARMERO
AND
KRISHNA GARIKIPATI

An Analysis of Strong Discontinuities in Multiplicative Finite Strain Plasticity and their Relation with the Numerical Simulation of Strain Localization in Solids

by

F. ARMERO[†] & K. GARIKIPATI[‡]

Structural Engineering, Mechanics and Materials,

Department of Civil Engineering,

University of California at Berkeley,

Berkeley CA, 94720

Dedicated to the memory of Juan C. Simo

Abstract

This paper presents an analysis of strong discontinuities in inelastic solids at finite strains. Solutions exhibiting this type of discontinuities, characterized by a discontinuous displacement field, are shown to make physical and mathematical sense in a classical multiplicative plasticity continuum model if the softening modulus is reinterpreted as a singular distribution. Physically, the softening is localized along the discontinuity. Conditions for the appearance of strong discontinuities in the geometrically nonlinear range are characterized, as it is the response of the material after localization. In addition, these analytical results are exploited in the design of a new class of finite element methods. The proposed methods fall within the class of enhanced strain methods, and lead to solutions independent of mesh size and insensitive to mesh alignment, without requiring any regulatization of the solutions by numerical parameters like a characteristic length.

1. Introduction.

The analysis of strain localization in inelastic materials has received an important amount of attention in the past, particularly in the last decade motivated by the interest in the numerical simulation of the failure of solids. Even though some of the physical and mathematical issues involved in this problem are already well understood, the problem can still be considered as open problem to a large extent, as pointed out recently in

---

[†] Assistant Professor of Civil Engineering, UC Berkeley.

[‡] Graduate Research Assistant, Stanford University

ZIENKIEWICZ [1992] . For instance, the presence of strain-softening in the constitutive law is known to be one of the factors that trigger the inception of strain localization. The mathematical inconsistencies that strain-softening may introduce in a continuum have been well characterized. These inconsistencies translate at the numerical level in the mesh dependence that finite element solutions exhibit. As described briefly below, a number of techniques have been proposed to overcome these inconsistencies, some of them leading to efficient numerical techniques. However, the appropriate choice seems still a matter of personal preference of the analyst.

Classical analyses of the localization in solids can be traced back to THOMAS [1961], HILL [1962] and MANDEL [1966], in connection with the earlier work of HADAMARD [1906] concerned with the study of discontinuities in solids. See also in this respect the complete analyses of RICE [1976] and ASARO [1983]. This approach is based on the consideration of the bifurcation of an homogeneous solution into a solution involving discontinuous deformation gradients. Such discontinuities are commonly referred to as *weak discontinuities*. The analysis identifies the *loss of strong ellipticity* of the governing equations of rate-independent models as a necessary condition for the appearance of such discontinuous solutions. Linearized stability analyses have been proposed for viscous models; see e.g. SHAWKI & CLIFTON for a comprehensive review article. Even though experimental results indicate the formation of very narrow bands, commonly known as shear bands, classical rate-independent plasticity models (like the one described in Section 2.2) do not possess an intrinsic characteristic length. As noted by Tresca as early as the end of last century (see the historical review of JOHNSON [1987]), at the macroscopic level it is appropriate to model the localization of strains by considering the limit case of a surface of discontinuity of the displacement field. The classical concept of a *slip-line*, as it appears in rigid-plastic theories is then recovered (see e.g. the classical texts of HILL [1950] or KACHANOV [1971]). The main goal of this paper is the precise characterization of this limit case, referred to as *strong discontinuities*, in the context of multiplicative finite strain plasticity.

A number of different approaches have been proposed in the literature that take into account the above considerations for the modeling of strain localization, with an especial interest in its numerical simulation. A first approach consists of the consideration of alternative constitutive models that possess an intrinsic characteristic length, regularizing the problem in the process. Examples of these ideas are non-local constitutive models (BAZANT et al [1984]), Cosserat type models (DE BORST & SLUYS [1991]), and higher-gradient models (COLEMAN & HODGON [1985]), to mention few representative references. There are a number of theoretical and practical issues that arise in these cases. Perhaps the most fundamental one is the actual definition (or rather determination) of the intrinsic characteristic length. At a more practical level, the extra numerical cost involved in these formulations over more traditional continuum models is sometimes difficult to justify.

A second traditional approach consists of the consideration of a numerical characteristic length for the regularization of the numerical simulations involving softening materials.

The standard continuum plasticity model is maintained, and the case of zero width of the localization band (now a surface) is assumed. However, a finite dissipation is associated to the deformation along the discontinuity. At the numerical level, more precisely in the context of the finite element method where the minimum width is determined by the size of the mesh, the dissipation per unit volume characteristic of a continuum material model is modified according to the size of the mesh to obtain a fixed and finite dissipation per unit area. Usually the slope of the (continuum) softening law is modified according to the mesh size through the introduction of the aforementioned characteristic length. In the limit, as the mesh size tends to zero, the localization surface is modeled by a discontinuity exhibiting a finite dissipation. See OLIVER [1989] for a precise discussion and formulation of these ideas. Similarly, the formulation of finite element methods incorporating special interpolation functions at the element level to capture the localization of the deformations can be found in BELYTSCHKO et al [1988] and NACAR et al [1989], to mention two representative examples.

An alternative approach was presented recently in SIMO, OLIVER & ARMERO [1993]. The main idea behind this approach is the consideration of the limit problem, i.e. solutions involving a discontinuous displacement field (*strong discontinuities*), in both the analysis and the development of numerical methods for the simulation of strain localization. Most notably, the analysis not only identifies the actual condition for the appearance of strong discontinuities (recovering in fact the loss of strong ellipticity condition), but also characterizes completely the localization mode. It is shown that to make mathematical and physical sense of the continuum equations a localized softening law along the discontinuity, relating the (driving) traction and jump of the displacement, is to be considered. It is therefore concluded the existence of a localized dissipation along the discontinuity. Finite element methods based on these ideas for the infinitesimal case have been presented in this last reference, SIMO & OLIVER [1994], and ARMERO & GARIKIPATI [1995]. The connection of these ideas with the previous approach based on a numerical characteristic length, as well as discrete crack type models (see e.g. HILLERBORG [1985]), becomes readily apparent. However, the different analytical characterization as well the completely different aspects involved in the numerical implementation of these theoretical results are to be contrasted.

We extend in this paper the ideas and results involved in this last approach to the fully nonlinear finite strain range. The main goal is to extract the information present in a classical continuum multiplicative plasticity model in order to characterize solutions involving strong discontinuities. The approach presented herein considers the bifurcation of a smooth initial solution into a solution involving strong discontinuities. The analysis then proceeds formally to make mathematical and physical sense of these equations in the context of distribution theory. Solutions exhibiting strong discontinuities are shown to be consistent with a rate-independent continuum model if the *strain-softening law is understood in distributional sense;* that is, the softening modulus is a singular distribution

(a delta function) along the discontinuity, meaning physically that the softening response of the material is localized in a set of measure zero.

It is important to note that a complete characterization of the functional setting of the problem is still a challenging open problem in the literature. In fact, even for the case of nonlinear elasticity there are still a number of open issues; see CIARLET [1988]. In the case of infinitesimal perfect plasticity, a key contribution was presented in MATTHIES et al. [1979], where the space of displacement fields with bounded (infinitesimal) deformations, the so-called $BD(\Omega)$ space, was identified in the context of the variational structure of the problem, as presented earlier in DUVAUT & LIONS [1972] and JOHNSON [1976]. Further results along these directions can be found in SUQUET [1978, 1981], TEMAM & STRANG [1980], ANZELLOTTI & GIAQUINTA [1982] and TEMAM [1986], among others. The approach proposed herein is a first formal attempt to extent these ideas to the finite strain range, and investigate their practical consequences in the design of finite element methods for the solution of the problem at hand.

At the numerical level, the main goal is not only the design of efficient numerical methods that are independent of the size of the mesh, but also the development of methods that are insensitive to the mesh alignment, despite the strong oriented character that localized solutions exhibit. The finite element methods proposed herein accomplish these features by the inclusion of the localization mode identified in the analysis of strong discontinuities in the actual finite element spaces, without resolving to a regularization of these discontinuities. The final methods are formulated in the context of the enhanced strain methodology proposed originally by SIMO & RIFAI [1990] in the infinitesimal range, and extended in SIMO & ARMERO [1992] and SIMO, ARMERO & TAYLOR [1993] to the geometrically nonlinear case. As a result, the finite element methods proposed herein do not require the introduction of any extra numerical parameters for a correct simulation of the localization of strains in inelastic solids.

An outline of the reminder of the paper is as follows. Section 2 defines the problem under consideration, introducing the notation used in the rest of the paper as well as a complete description of the constitutive equations characterizing multiplicative finite strain plasticity. Section 3 includes the analysis of strong discontinuities in this fully nonlinear range. A description of the kinematics of this class of discontinuities as well as the conditions for their appearance in inelastic solids is presented. A complete characterization of the localization mode is similarly obtained. These theoretical results are exploited in Section 4 in the design of a new class of enhanced strain finite element methods. A brief description of these methods is presented, together with the discussion of a representative numerical simulation showing the main properties of the proposed methods. Finally, concluding remarks are drawn in Section 5.

2. Problem Definition.

This section describes the governing equations of the problem under consideration. The notation employed in the rest of the paper is introduced as well.

2.1. Governing Equations. Notation.

Let $\mathcal{B} \subset \mathbb{R}^{n_{\dim}}$ ($n_{\dim} = 1, 2$ or 3) be the reference placement of a solid with material particles denoted by $\boldsymbol{X} \in \mathcal{B}$. Let the solid be subjected to a deformation $\boldsymbol{\varphi}: \mathcal{B} \to \mathbb{R}^{n_{\dim}}$, with $\det D\boldsymbol{\varphi} > 0$ and satisfying the essential boundary conditions $\boldsymbol{\varphi} = \hat{\boldsymbol{\varphi}}$ on $\partial_u \mathcal{B} \subset \partial \mathcal{B}$ for some given function $\hat{\boldsymbol{\varphi}}$. Denote by $\boldsymbol{P}$ the nominal stress field (first Piola-Kirchhoff stress tensor), defined by the particular constitutive relations of the material as described in the following section.

In this context, the weak form of the equilibrium equations are given by the usual expression

$$\int_{\mathcal{B}} \boldsymbol{P} : \mathrm{GRAD}[\boldsymbol{\eta}] \, d\mathcal{B} = \int_{\mathcal{B}} \boldsymbol{f} \cdot \boldsymbol{\eta} \, d\mathcal{B} + \int_{\partial_t \mathcal{B}} \hat{\boldsymbol{T}} \cdot \boldsymbol{\eta} \, d\Gamma \qquad \forall \boldsymbol{\eta} \in \mathcal{V}_o \, , \tag{2.1}$$

for a given body force field $\boldsymbol{f}$ and imposed tractions $\hat{\boldsymbol{T}}$ on $\partial_t \mathcal{B} \subset \partial \mathcal{B}$. The usual assumptions

$$\overline{\partial_u \mathcal{B} \cup \partial_t \mathcal{B}} = \partial \mathcal{B} \qquad \text{and} \qquad \partial_u \mathcal{B} \cap \partial_t \mathcal{B} = \varnothing \, , \tag{2.2}$$

are considered. The space of test functions $\mathcal{V}_o$ is defined as

$$\mathcal{V}_o := \{ \boldsymbol{\eta}: \mathcal{B} \to \mathbb{R}^{n_{\dim}} \quad : \quad \boldsymbol{\eta} = 0 \quad \text{on} \quad \partial_u \mathcal{B} \} \tag{2.3}$$

with the appropriate smoothness conditions for (2.1) to make sense. It is to be noted in this respect that even for the case of hyperelasticity where there is a complete existence and regularity theory for $\boldsymbol{\varphi}$ as a minimizer of the potential energy (BALL [1977]), it is not clear in what sense the weak Euler-Lagrange equations (2.1) are satisfied. The reader is referred to CIARLET [1988], Section 7.10, for further details.

Let $\Gamma \subset \mathcal{B}$ denote a smooth (C^1) surface in $\mathbb{R}^{n_{\dim}-1}$ with unit normal $\boldsymbol{N}$. Assume that $\boldsymbol{P}$ is everywhere continuous, except perhaps across Γ. Then, a calculation based on integration by parts in (2.1) leads to

$$\int_{\mathcal{B}} [\mathrm{DIV}[\boldsymbol{P}] + \boldsymbol{f}] \cdot \boldsymbol{\eta} \, d\mathcal{B} + \int_{\Gamma} [\![\boldsymbol{P}]\!] \boldsymbol{N} \cdot \boldsymbol{\eta} \, d\Gamma + \int_{\partial_t \mathcal{B}} [\hat{\boldsymbol{T}} - \boldsymbol{P}\boldsymbol{N}] \cdot \boldsymbol{\eta} \, d\Gamma \, , \qquad \forall \boldsymbol{\eta} \in \mathcal{V}_o$$

where $[\![\boldsymbol{P}]\!]$ denotes the jump of the stresses $\boldsymbol{P}$ across Γ. A classical argument leads then to the local (strong) form of the equilibrium equations and natural boundary conditions, i.e.

$$\mathrm{DIV}[\boldsymbol{P}] + \boldsymbol{f} = 0 \qquad \text{and} \qquad \boldsymbol{P}\boldsymbol{N} = \hat{\boldsymbol{T}} \quad \text{on} \quad \partial_t \mathcal{B} \, , \tag{2.4}$$

together the compatibility jump condition

$$[\![P]\!]N = 0 \quad \text{on} \quad \Gamma \, .\tag{2.5}$$

This result allows to introduce a well-defined object $T_\Gamma := PN$ on Γ, which we shall refer to as the *nominal driving traction*.

2.2. Constitutive relations.

This section introduces the constitutive equations considered in the present analysis, namely, finite strain multiplicative plasticity. A very brief summary is given in Section 2.2.1 of the relations characterizing this class of constitutive models. The reader is referred to the comprehensive monograph by SIMO [1995] for further details. The elastic rate equations employed in the forthcoming analysis are derived in Section 2.2.2.

2.2.1. Multiplicative finite strain plasticity.

The case of interest corresponds to a rate-independent plasticity model, characterized by the multiplicative decomposition

$$F = F^e F^p \, ,\tag{2.6}$$

of the deformation gradient $F := D\varphi$ in an elastic F^e and a plastic part F^p. In this context, a general plasticity model is characterized by the following constitutive relations.

i. *Hyperelastic response.* The elastic response of the material is characterized by a stored energy function

$$W = \hat{W}(C^e) \quad \text{with} \quad C^e := F^{eT} F^e \, ,\tag{2.7}$$

where the dependence on C^e follows from a classical argument based on material frame indifference. The stresses in the material are then given by the relations

$$S = 2\partial_{C^e} W \quad \text{and} \quad \tau = F^e \, S \, F^{eT} \, ,\tag{2.8}$$

where S is the second Piola-Kirchhoff stress tensor (in the intermediate local configuration defined by F^p), with $P = F^e S$ and the Kirchhoff stresses τ. Recall that the Cauchy stresses (true stresses) σ are given by $\sigma := \tau/J$ with $J := \det F > 0$.

ii. *Yield condition.* We consider a model determined by an admissible elastic domain defined in terms of the Kirchhoff stresses τ, given by a *yield function* of the form

$$\phi(\tau, q) = \hat{\phi}(\tau) + q - \sigma_y \leq 0 \, ,\tag{2.9}$$

where q denotes a scalar stress-like internal variable modeling the hardening/softening response of the material. Relation (2.9) represents a typical yield surface with an initial yield limit σ_y, and a homogeneous function $\hat{\phi}(\boldsymbol{\tau})$ of degree one. It is to be noted that relation (2.9) is restricted to the isotropic case by frame indifference

$$\hat{\phi}(\boldsymbol{Q}\boldsymbol{\tau}\boldsymbol{Q}^T) = \hat{\phi}(\boldsymbol{\tau}) \qquad \forall \boldsymbol{Q} \in SO(n_{\text{dim}}) , \tag{2.10}$$

i.e., $\hat{\phi}(\boldsymbol{\tau})$ is an *isotropic* function of the Kirchhoff stresses $\boldsymbol{\tau}$. We shall restrict the following developments to this case for simplicity.

ii. *Plastic evolution equations.* The use of the decomposition (2.6) results in the additive decomposition

$$\boldsymbol{l} := \dot{\boldsymbol{F}}\boldsymbol{F}^{-1} = \underbrace{\dot{\boldsymbol{F}}^e\boldsymbol{F}^{e-1}}_{:= \, \boldsymbol{l}^e} + \underbrace{\boldsymbol{F}^e\dot{\boldsymbol{F}}^p\boldsymbol{F}^{p-1}\boldsymbol{F}^{e-1}}_{:= \, \boldsymbol{F}^e\boldsymbol{L}^p\boldsymbol{F}^{e-1} \, := \, \boldsymbol{l}^p} = \boldsymbol{l}^e + \boldsymbol{l}^p , \tag{2.11}$$

for the spatial velocity gradient tensor $\boldsymbol{l}$. The evolution equations of the plastic rate of the deformation and plastic spin are given in general by

$$\boldsymbol{d}^p := \text{sym}\,(\boldsymbol{l}^p) = \lambda\,\boldsymbol{n}_\phi , \qquad \text{and} \qquad \boldsymbol{\omega}^p := \text{skew}\,(\boldsymbol{l}^p) = \lambda\,\hat{\boldsymbol{\omega}} , \tag{2.12}$$

where $0 \leq \lambda \in \mathbb{R}$ is the *plastic consistency parameter*, and the symmetric tensor $\boldsymbol{n}_\phi$ and skew-symmetric tensor $\hat{\boldsymbol{\omega}}$ are two given tensors defining the evolution of the plastic deformation rate and plastic spin, respectively. It is to be noted that both $\boldsymbol{d}^p$ and $\boldsymbol{\omega}^p$ are objective rates, so the constitutive relations (2.12) are correctly defined. Typically the plastic spin is assumed to vanish $\hat{\boldsymbol{\omega}} = 0$; see MOHAN, ORTIZ & SHIH [1990], SIMO [1995], and references therein. See DAFALIAS [1984], and ANAND [1985] for examples involving a non-zero plastic spin. We shall restrict the following developments to the case characterized by

$$\boldsymbol{n}_\phi = \partial_{\boldsymbol{\tau}}\phi(\boldsymbol{\tau}, q) , \tag{2.13}$$

that is, $\boldsymbol{n}_\phi$ is the normal to the yield surface. Similarly, we shall consider an associated hardening/softening law given by

$$H^{-1}\,\dot{q} = -\lambda\,\partial_q\phi = -\lambda , \tag{2.14}$$

for a *hardening/softening modulus H*.

iii. *Kuhn-Tucker conditions.* The elastoplastic model is completely defined then by the conditions

$$\phi \leq 0 , \qquad \lambda \geq 0 , \qquad \lambda\phi = 0 , \qquad \text{and} \qquad \lambda\dot{\phi} = 0 , \tag{2.15}$$

identifying the loading/unloading conditions.

Remark 2.1. An important consequence of the choice (2.13) will be used in the forthcoming developments. Since $\phi(\cdot, q)$ is an isotropic function of τ by (2.10), the two symmetric tensors n_ϕ and τ are coaxial. Therefore, these two tensors commute, $n_\phi \tau$ is symmetric, and consequently

$$n_\phi : w\tau = n_\phi : \tau w = 0 \tag{2.16}$$

for all skew-symmetric tensors $w \in so(n_{\text{dim}})$. ∎

2.2.2. Rate form of the elastic constitutive relations.

We conclude this section with the derivation the rate form of the elastic relations considered above. Taking the material time derivative of $(2.8)_1$ and making use of the relation $\frac{1}{2}\dot{C}^e = F^e d^e F^{eT}$, we obtain

$$\dot{S} = \mathbb{C}_e \frac{1}{2}\dot{C}^e \quad \Longleftrightarrow \quad \mathcal{L}_v^e \tau := F^e \dot{S} F^{eT} = \mathbf{c}_e d^e , \tag{2.17}$$

where the material $\mathbb{C}_e$ and spatial $\mathbf{c}_e$ elastic moduli are defined by

$$\mathbb{C}_e^{IJKL} = 4\frac{\partial^2 W}{\partial C_{IJ}^e \partial C_{KL}^e} \quad \text{and} \quad \mathbf{c}_e^{ijkl} = F^{ei}_{\ I} F^{ej}_{\ J} F^{ek}_{\ K} F^{el}_{\ L} \mathbb{C}_e^{IJKL} , \tag{2.18}$$

respectively. Given $(2.18)_1$, the spatial elastic tangent tensor $\mathbf{c}_e$ possesses the minor symmetries

$$\mathbf{c}_e^{ijkl} = \mathbf{c}_e^{jikl} = \mathbf{c}_e^{ijlk} , \tag{2.19}$$

and the major symmetry

$$\mathbf{c}_e^{ijkl} = \mathbf{c}_e^{klij} . \tag{2.20}$$

Expanding the material time derivative in $(2.17)_2$ using (2.8), we obtain the equivalent expression

$$\mathcal{L}_v^e \tau = \dot{\tau} - l^e \tau - \tau l^{eT} , \tag{2.21}$$

for the elastic Lie derivative of the Kirchhoff stresses.

The elastic rate equations can also be expressed in terms of the elastic Jaumann rate of the Kirchhoff stresses $\overset{\nabla_e}{\tau}$, defined as

$$\overset{\nabla_e}{\tau} := \dot{\tau} - \omega^e \tau - \tau \omega^{eT} = \mathcal{L}_v^e \tau + d^e \tau + \tau d^{eT} , \tag{2.22}$$

where ω^e denotes the elastic spin $\omega^e := \text{skew}[l^e]$. Combining this last expression with (2.18) leads to the relation

$$\overset{\nabla_e}{\tau} = \mathbf{a}_e d^e , \quad \text{where} \quad \mathbf{a}_e^{ijkl} = \mathbf{c}_e^{ijkl} + \frac{1}{2}\left[\tau^{ik}\delta^{jl} + \tau^{il}\delta^{jk}\right] + \frac{1}{2}\left[\tau^{jl}\delta^{ik} + \tau^{jk}\delta^{il}\right] . \tag{2.23}$$

after some straightforward algebraic manipulations. The spatial tangent $\mathbf{a}_e$ possesses the same symmetries (2.19)-(2.20) as $\mathbf{c}_e$.

Remark 2.2. The different character of the yield condition (2.9) when compared with the rest of the equations defining the constitutive model should be noted. Namely, (2.9) is a pointwise bound on the stresses τ and q. This fact can be easily seen for the case $\hat{\omega} = 0$ by casting the model in the form of a variational inequality. Using the notation introduced in this section, and after some straightforward algebraic manipulations, we arrive at the expression

$$\int_{\mathcal{B}} \left[(\tau - \tilde{\tau}) \left(\nabla v - \mathbf{a}_e^{-1} \overset{\nabla}{\tau} \right) - (q - \tilde{q}) \; H^{-1} \; \dot{q} \right] \; d\mathcal{B} \le 0 \qquad \forall (\tilde{\tau}, \tilde{q}) \in \mathbb{E} \;, \tag{2.24}$$

where $v := \dot{\varphi}$ is the material velocity, and $\mathbb{E} = \left\{ (\tau, q) \in \mathbb{S} \times \mathbb{R} : \; \phi(\tau, q) \le 0 \right\}$ (with $\mathbb{S}$ being the space of rank two symmetric tensors) is the (pointwise) *elastic admissible domain* defined by (2.9). Note that in this case $\overset{\nabla}{\tau} = \overset{\nabla_e}{\tau}$, since $\omega^p \equiv 0$. The reader is referred to SIMO [1995] for a complete description of the details involved in (2.24). In particular, the variational principle underlying (2.24) corresponds to the classical *principle of maximum plastic dissipation*. ∎

3. Strong Discontinuities in Multiplicative Plasticity.

This section describes the conditions that govern the appearance of strong discontinuities in the context of the general class of multiplicative plasticity models summarized in the previous section. The approach considered herein follows the classical analysis of weak discontinuities as a bifurcation problem from an homogeneous deformation state. We consider, however, the limiting problem involving a *strong discontinuity* (a discontinuity of the deformation φ itself). To this purpose, the kinematics of strong discontinuities in the finite strain range are described first.

3.1. Kinematics of strong discontinuities.

Consider an initial deformation $\bar{\varphi} : \mathcal{B} \to \mathbb{R}^{n_{\dim}}$, assumed smooth in $\mathcal{B}$, with a (regular) deformation gradient $\bar{F} = D\bar{\varphi}$. We want to investigate the conditions that make possible the bifurcation of this field to a *discontinuous* or *singular* deformation across a smooth material surface $\Gamma \subset \mathcal{B} \cap \mathbb{R}^{n_{\dim}-1}$ in a neighborhood $\Omega_\Gamma \subset \mathcal{B}$ of a point $X_\Gamma \in \mathcal{B}$. With no loss of generality we may assume $\bar{\varphi}$ to be homogeneous in Ω_Γ. Consider then the discontinuous deformation in Ω_Γ defined by

$$\varphi(X) = \bar{\varphi}(X) + [\![\varphi]\!] \; H_\Gamma(X) \;, \qquad \forall X \in \Omega_\Gamma \tag{3.1}$$

where $[\![\varphi]\!] : \mathcal{B} \to \mathbb{R}^{n_{\dim}}$ is the jump discontinuity, and $H_\Gamma(X)$ denotes the Heaviside function on Γ, i.e.

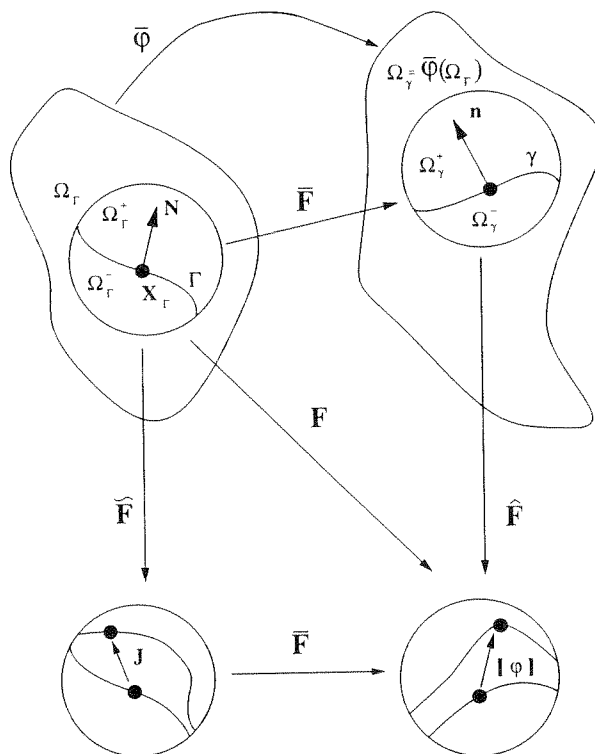$$H_\Gamma(X) = \begin{cases} 1 & \text{if } X \in \Omega_\Gamma^+ \;, \\ 0 & \text{if } X \in \Omega_\Gamma^- \;. \end{cases} \tag{3.2}$$

FIGURE 3.1. Kinematics of strong discontinuities. Local decompositions associated to a strong discontinuity

Here, Ω_Γ^+ and Ω_Γ^- denote the components of Ω_Γ on either side of the surface Γ; see Figure 3.1. Denote by $\boldsymbol{N}$ the unit normal to Γ (pointing to Ω_Γ^+). It is to be noted that Γ needs only to be defined locally in the neighborhood Ω_Γ. Given the assumed smoothness of Γ, there would be then no loss of generality in restricting the following argument to a plane through $\boldsymbol{X}_\Gamma$ with normal $\boldsymbol{N}$. Similarly, the decomposition (3.1) is defined locally. The relations obtained from this analysis are *necessary local conditions* for the appearance of strong discontinuities in solids.

The deformation gradient $\boldsymbol{F}$ corresponding to the deformation $\boldsymbol{\varphi}(\boldsymbol{X})$ in (3.1) is given, after using a classical result in distribution theory, by

$$\boldsymbol{F} = \bar{\boldsymbol{F}} + [\![\boldsymbol{\varphi}]\!] \otimes \boldsymbol{N} \, \delta_\Gamma \,, \tag{3.3}$$

where δ_Γ denotes the *Dirac delta function* on Γ. We introduce the *material jump* $\boldsymbol{J} : \mathcal{B} \to \mathbb{R}^{n_{\dim}}$, defined by

$$\boldsymbol{J} := \bar{\boldsymbol{F}}^{-1}[\![\boldsymbol{\varphi}]\!] \,, \tag{3.4}$$

i.e., the pull-back of the spatial jump $[\![\boldsymbol{\varphi}]\!]$ by the original smooth deformation. With this notation in hand, the singular deformation gradient $\boldsymbol{F}$ in (3.3) can be written as

$$\boldsymbol{F} = \bar{\boldsymbol{F}}\tilde{\boldsymbol{F}} \qquad \text{where} \quad \tilde{\boldsymbol{F}} := 1 + \boldsymbol{J} \otimes \boldsymbol{N} \, \delta_\Gamma \,. \tag{3.5}$$

This last relation introduces a multiplicative decomposition of the total deformation gradient $\boldsymbol{F}$ in a regular $\bar{\boldsymbol{F}}$ and singular part $\tilde{\boldsymbol{F}}$.

The above material description of the discontinuous deformation under investigation has a spatial counterpart. To this purpose, denote by $\gamma = \bar{\varphi}(\Gamma)$ the current placement of the material surface Γ. Then, the deformation gradient $\boldsymbol{F}$ associated to the discontinuous mode (3.1) can be decomposed equivalently as

$$\boldsymbol{F} = \hat{\boldsymbol{F}}\bar{\boldsymbol{F}} \qquad \text{where} \quad \hat{\boldsymbol{F}} = 1 + [\![\varphi]\!] \otimes \boldsymbol{n}\,\delta_\Gamma \,, \tag{3.6}$$

and where $\boldsymbol{n}$ denotes the normal to the surface γ obtained as

$$\boldsymbol{n} = \bar{\boldsymbol{F}}^{-T}\boldsymbol{N} \,. \tag{3.7}$$

The vector $\boldsymbol{n}$ is normal to γ at $\varphi(\boldsymbol{X}_\Gamma)$, but it need not be a unit vector necessarily. Note also that we can write $\bar{J}\delta_\Gamma = \delta_\gamma$, where δ_γ denotes the Dirac delta function on γ and $\bar{J} := \det\bar{\boldsymbol{F}} > 0$. The multiplicative decompositions (3.5) and (3.6) are illustrated in Figure 3.1.

The next step is the calculation of the velocity gradient tensor associated with the bifurcation to the discontinuous mode φ in (3.1) from the original smooth deformation $\bar{\varphi}$. An argument similar to (2.11) involving the decomposition (3.5)$_1$ and the material character of the surface S (i.e., $\dot{\boldsymbol{N}} = 0$), leads readily to

$$\begin{aligned}
\boldsymbol{l} := \dot{\boldsymbol{F}}\boldsymbol{F}^{-1}\Big|_{\boldsymbol{F}=\bar{\boldsymbol{F}}} &= \dot{\bar{\boldsymbol{F}}}\bar{\boldsymbol{F}}^{-1} + \bar{\boldsymbol{F}}\dot{\hat{\boldsymbol{F}}}\bar{\boldsymbol{F}}^{-1} \\
&= \dot{\bar{\boldsymbol{F}}}\bar{\boldsymbol{F}}^{-1} + \bar{\boldsymbol{F}}[\![\dot{\varphi}]\!] \otimes \bar{\boldsymbol{F}}^{-T}\boldsymbol{N}\,\delta_\Gamma \\
&= \bar{\boldsymbol{l}} + \boldsymbol{\mathcal{L}}_v[\![\varphi]\!] \otimes \boldsymbol{n}\,\delta_\Gamma \\
&= \bar{\boldsymbol{l}} + \tilde{\boldsymbol{l}} \,,
\end{aligned} \tag{3.8}$$

where we have introduced the spatial objects

$$\bar{\boldsymbol{l}} := \dot{\bar{\boldsymbol{F}}}\bar{\boldsymbol{F}}^{-1} \,, \qquad \tilde{\boldsymbol{l}} := \boldsymbol{\mathcal{L}}_v[\![\varphi]\!] \otimes \boldsymbol{n}\,\delta_\Gamma \,, \qquad \text{and} \quad \boldsymbol{\mathcal{L}}_v[\![\varphi]\!] := \bar{\boldsymbol{F}}\dot{\hat{}} \,. \tag{3.9}$$

Relation (3.9)$_3$ identifies $\boldsymbol{\mathcal{L}}_v[\![\varphi]\!]$ with the Lie derivative of the jump vector $[\![\varphi]\!]$. A simple calculation shows the important fact that this object is frame indifferent; that is, given two observers related by a rigid body motion, we have

$$\text{if} \quad \bar{\boldsymbol{F}}^* = \boldsymbol{Q}\bar{\boldsymbol{F}} \,, \quad \text{then} \quad \boldsymbol{\mathcal{L}}_v[\![\varphi]\!]^* = \boldsymbol{Q}\boldsymbol{\mathcal{L}}_v[\![\varphi]\!] \,, \quad \forall \boldsymbol{Q} \in SO(n_{\text{dim}}) \,. \tag{3.10}$$

Therefore, we conclude that the appearance of the bifurcation to the discontinuous mode (3.1) leads to an additive decomposition (3.8) of the spatial velocity gradient $\boldsymbol{l}$ in a regular $\bar{\boldsymbol{l}}$ and singular part $\tilde{\boldsymbol{l}}$ on the discontinuity Γ, the latter being an objective rate tensor (since

both $\mathcal{L}_v[\![\varphi]\!]$ and n are objective). Outside the discontinuity (i.e., in $\Omega_\Gamma\backslash\Gamma$) the material is subjected to the bounded velocity gradient $\bar{l}$. Remarkably, as in the case of weak discontinuities characterized by a continuous deformation and discontinuous deformation gradients, the difference between the basis and bifurcated modes involves a rank one tensor. However, the singular character of $\tilde{l}$ in $(3.9)_2$ is to be noted.

Remark 3.1. It is important to emphasize once again the *local* character assumed for the decomposition (3.1). Figure 3.1 has to be understood in a local sense. For instance, the two surfaces that may appear after the inception of the discontinuous solution will not be considered in the actual numerical simulations. Alternatively, a constitutive relation will be derived for the jump $[\![\varphi]\!]$ modeling the localized response of the material. For this purpose, the objectivity of the strain rate $\mathcal{L}_v[\![\varphi]\!]$ pointed out above will prove to be crucial, as shown in the next section. ∎

3.2. Strain localization in multiplicative plasticity.

This section investigates the conditions that make possible the discontinuous deformation (3.1) in the general class of multiplicative plasticity model described in Section 2. For this purpose, the assumptions considered in the analysis are first characterized in Section 3.2.1. The localization condition signaling the appearance of localization is derived in Section 3.2.2. A complete characterization of the localization mode is obtained in Section 3.2.3.

3.2.1. Basic assumptions.

From a theoretical point of view, the two main assumptions underlying the approach described herein are:

1. The continuum constitutive model prior to localization is able to predict the inception of the localization of the strains.

2. Moreover, the localization mode is characterized by the rate relations of the continuum model, i.e. persistency of the continuum relations is imposed during localization.

It is to be noted that these assumptions are also considered in classical analyses involving weak discontinuities. Assumption 1 can be found stated explicitly in RICE [1976]. Physically, these assumptions imply that even though the actual physical mechanism controlling the material response after localization may be completely different that the physical mechanisms responsible for the response of the solid prior to the bifurcation, localization can be signaled and described by the relations of the continuum model.

For the case of interest here, involving strong discontinuities with the corresponding strain rates being singular distribution as described in the previous section, Assumption

2 implies that the continuum rate equations have to make physical and mathematical sense in general distributional form. To this end, and given the character of the different equations described in Section 2, we have:

1. To make sense of the *pointwise constraint* imposed by the yield condition (2.9) (see Remark 2.2), the stress-like variables q and the function $\hat{\phi}(\boldsymbol{\tau})$ of the Kirchhoff stress $\boldsymbol{\tau}$ are (pointwise) *bounded functions* in $\mathcal{B}$. Technically, these functions are $C^0(\mathcal{B})$; see e.g. MATHIES et al. [1979] for a discussion in the infinitesimal range.

2. Persistency of the boundedness conditions identified in the previous item implies that $\dot{q}$ and $\dot{\hat{\phi}}(\boldsymbol{\tau})$ remain regular functions (that is, they are not singular distributions), making sense of the consistency condition $(2.15)_4$ in the case of plastic flow.

3. Similarly, the nominal traction $\boldsymbol{T}_\Gamma$ is continuous by the equilibrium equations, as obtained in (2.5), and remains bounded. Therefore, $\dot{\boldsymbol{T}}_\Gamma$ is not a singular distribution.

The above considerations for the stress-like variables in the model are to be contrasted with the singular character of the strain rate measures as described in the previous section. In particular, the plastic consistency parameter determining the plastic rates will be in general a singular distribution. Note that evolution tensors $\boldsymbol{n}_\phi$ and $\hat{\boldsymbol{\omega}}$ in (2.12) are bounded objects depending on the smooth deformation $\bar{\boldsymbol{\varphi}}$. The case of interest herein involves localized plastic flow along the discontinuity. We referred to this case as the *localization mode* on Γ, being characterized by

$$\lambda = \lambda_\Gamma \, \delta_\Gamma \ , \tag{3.11}$$

with $\lambda_\Gamma > 0$ by $(2.15)_2$. The regular part of λ is associated to diffusive plastic flow outside the discontinuity, leading to standard treatments of the plasticity problem. Therefore, and without loss of generality, this part is assumed to vanish in (3.11) and in the following developments.

The goal of the analysis presented in the following sections is to make physical and mathematical sense of the constitutive relations given the above considerations. The main objective is to identify not only the conditions that indicate the appearance of the localized mode defined by (3.11), but also to characterize completely this mode. In particular, the evolution of the jump $[\![\boldsymbol{\varphi}]\!]$ is of the main interest.

3.2.2. The localization condition in multiplicative plasticity.

The first step in the analysis is to obtain the explicit expression of the evolution of the nominal traction $\boldsymbol{T}_\Gamma$ on Γ. For this purpose, we note that

$$\dot{\boldsymbol{T}}_\Gamma = \dot{\boldsymbol{P}}\boldsymbol{N} = \left[\boldsymbol{\mathcal{L}}_v\boldsymbol{\tau} + l\boldsymbol{\tau}\right]\boldsymbol{n} = \left[\boldsymbol{\mathcal{L}}_v^e\boldsymbol{\tau} - l^p\boldsymbol{\tau} - \boldsymbol{\tau}l^{pT} + l\boldsymbol{\tau}\right]\boldsymbol{n}$$

$$= \left[\mathsf{c}_e d^e - l^p \tau - \tau l^{pT} + l\tau \right] n$$

$$= \left[\mathsf{c}_e d - \mathsf{a}_e d^p - \omega^p \tau - \tau \omega^{pT} + l\tau \right] n$$

$$= \underbrace{\left[\mathsf{c}_e \bar{d} + \bar{l}\tau \right] n}_{regular} + \underbrace{\left[\mathsf{c}_e \tilde{d} - \mathsf{a}_e \tilde{d}^p - \tilde{\omega}^p \tau - \tau \tilde{\omega}^{pT} + \tilde{l}\tau \right] n}_{singular} , \qquad (3.12)$$

after noting that N is a material vector (i.e. $\dot{N} = 0$). Here, the decomposition of the symmetric strain rate tensor

$$d := \mathrm{sym}[l] = \bar{d} + \tilde{d} , \qquad \text{where} \qquad \bar{d} := \mathrm{sym}[\bar{l}] \qquad \text{and} \qquad \tilde{d} := \mathrm{sym}[\tilde{l}] , \qquad (3.13)$$

have been introduced after the decomposition (3.8) of l. Similarly, $\tilde{d}^p = d^p$ and $\tilde{\omega}^p = \omega^p$ given the singular character of λ by (3.11). Impose that $\dot{T}_\Gamma$ is a regular function, i.e. the singular part of (3.12) must vanish, leading to

$$\left[\mathsf{c}_e \tilde{d} - \mathsf{a}_e \tilde{d}^p - \tilde{\omega}^p \tau - \tau \tilde{\omega}^{pT} + \tilde{l}\tau \right] n = 0 . \qquad (3.14)$$

Setting $\tilde{d}^p = \lambda n_\phi$ and $\tilde{\omega}^p = \lambda \hat{\omega}$, equation (3.14) can be written as

$$\left[\mathsf{c}_e \tilde{d} - \lambda (\mathsf{a}_e n_\phi + \tau \hat{\omega} - \hat{\omega}\tau) + \tilde{l}\tau \right] n = 0 . \qquad (3.15)$$

It is to be noted that both $\tilde{d}$ and λ are singular distributions proportional to δ_Γ.

Next, the plastic consistency condition (2.15)$_4$ leads to

$$0 = \dot{\phi} = n_\phi : \dot{\tau} + \dot{q} = n_\phi : \overset{\triangledown_e}{\tau} + \dot{q} = n_\phi : \mathsf{a}_e (d - d^p) + \dot{q}$$

$$= \underbrace{n_\phi : \mathsf{a}_e \bar{d} + \dot{q}}_{regular} + \underbrace{n_\phi : \mathsf{a}_e (\tilde{d} - \tilde{d}^p)}_{singular} , \qquad (3.16)$$

where the result (2.16) has been used explicitly. The regularity conditions described in the previous section allow to identify the regular and singular components of this last expression. The two parts must vanish separately for the plastic consistency condition to make sense, leading to

$$n_\phi : \mathsf{a}_e \bar{d} + \dot{q} = 0 , \qquad (3.17)$$

and

$$n_\phi : \mathsf{a}_e (\tilde{d} - \tilde{d}^p) = 0 \quad \Rightarrow \quad \lambda = \frac{1}{n_\phi : \mathsf{a}_e n_\phi} n_\phi : \mathsf{a}_e \tilde{d} . \qquad (3.18)$$

for the singular plastic consistency paramenter $\lambda = \lambda_\Gamma \delta_\Gamma$.

Combining (3.15) and (3.18), and noting that $\tilde{l} = \mathcal{L}_v[\varphi] \otimes n \, \delta_\Gamma$ with $\tilde{d} = \mathrm{sym}(\tilde{l})$, we conclude that the $\mathcal{L}_v[\varphi]$ must satisfy the equation

$$\boxed{Q_{ep} \mathcal{L}_v[\varphi] = 0} \qquad (3.19)$$

where

$$Q_{ep} = n \cdot \left[\mathbf{c}_e - \frac{1}{n_\phi : \mathbf{a}_e n_\phi} (\mathbf{a}_e n_\phi + \tau \hat{\omega} - \hat{\omega}\tau) \otimes \mathbf{a}_e n_\phi \right] n + (n \cdot \tau n)\,\mathbf{1}\,, \qquad (3.20)$$

with $\mathbf{1}$ behind the rank two identity tensor. Condition (3.19) has the classical form of the *loss of (strong) ellipticity condition* (see TRUESDELL & NOLL [1965]), involving though the *acoustic tensor* Q_{ep} constructed with the *perfect plasticity* tangent tensor (the bracketed expression in (3.20)). In fact, repeating the same argument for the case of λ being a regular function (i.e. no localization of the plastic flow), condition (3.19) is obtained, involving now the elastic acoustic tensor

$$Q_e = n \cdot \mathbf{c}_e n + (n \cdot \tau n)\,\mathbf{1}\,, \qquad (3.21)$$

or, in index notation, $Q_e^{ik} = n_j\, c_e^{ijkl} n_l + \tau^{jl} n_j n_l \delta^{ik}$. In what follows, we shall assume that the elastic law does not exhibit the loss of ellipticity, focusing on the localization mode (3.11) triggered by the inelastic response of the material.

In summary, a necessary local condition for the bifurcation to a discontinuous deformation under the assumptions indicated in the previous section is that the *perfectly plastic acoustic tensor* is singular, with $\pounds_v[\![\varphi]\!]$ belonging to the kernel of Q^{ep}. This condition is the analog to the result obtained in SIMO, OLIVER & ARMERO [1993] for the infinitesimal case. We shall refer to this condition as the *localization condition*.

3.2.3. The localization mode.

The goal of this section is to characterize the discontinuous mode of the deformation that may appear when the localization condition (3.19) is satisfied for some N (or corresponding n). To this purpose, the hardening/softening law (2.14) together with the fact that $\dot{q}$ is a regular function as indicated in the previous section, imply the result

$$H^{-1} \underbrace{\dot{q}}_{regular} = \underbrace{-\lambda_\Gamma\,\delta_\Gamma}_{singular\ distribution} \qquad \Longrightarrow \qquad \boxed{H^{-1} = \bar{H}^{-1}\,\delta_\Gamma\,.} \qquad (3.22)$$

That is, a *distributional softening response* localized on the discontinuity surface Γ is obtained. See Remark 3.2 below for a justification of the claim that the localized plastic flow must involve a softening response in these circumstances. The same conclusion has been obtained in SIMO, OLIVER & ARMERO [1993] in the infinitesimal problem, with a direct relation of $\bar{H}$ with the energy expended in the material to create the discontinuity surface ('fracture' energy). The reader is referred to this last reference for further details.

The regular part of the consistency condition given by (3.17) leads to the relation

$$0 = n_\phi : \mathbf{a}_e \bar{d} + \dot{q} = n_\phi : \overset{\nabla_e}{\tau} + \dot{q}\,, \qquad (3.23)$$

where $\overset{\nabla e}{\tau} = \mathbf{a}_e \bar{d}$ is the elastic stress response outside the discontinuity Γ. Therefore, we can write

$$\dot{q} = -\bar{H}\lambda_\Gamma = -\mathbf{n}_\phi : \overset{\nabla e}{\tau} , \qquad (3.24)$$

where we have made use of (3.22). The combination of this equation with (3.18) implies that the strength of the rate of the jump ζ, defined by

$$\pounds_v [\![\boldsymbol{\varphi}]\!] =: \zeta\, \mathbf{m} \qquad \text{with} \qquad \|\mathbf{m}\| = 1 , \qquad (3.25)$$

is obtained as

$$\boxed{\zeta = \frac{1}{\Xi\bar{H}}\mathbf{n}_\phi : \overset{\nabla e}{\tau}\Big|_\Gamma} \qquad \Xi := \frac{\mathbf{a}_e\mathbf{n}_\phi : (\mathbf{n} \otimes \mathbf{m})^s}{\mathbf{n}_\phi : \mathbf{a}_e\mathbf{n}_\phi} . \qquad (3.26)$$

Therefore, we conclude that the rate of the jump is given directly in terms of the localized softening modulus $\bar{H}$, and the elastic evolution of the stresses $\overset{\nabla e}{\tau}$ outside the band.

Remark 3.2. The localization mode is characterized by elastic unloading outside Γ, since the regular part of λ vanishes by (3.11). The Kuhn-Tucker loading/unloading conditions (2.15) can be written equivalently in the classical form $\mathbf{n}_\phi : \overset{\nabla e}{\tau} \leq 0$ in this case. This relation together with the consistency relation (3.24) lead to $\dot{q} \geq 0$, which together with $\lambda_\Gamma > 0$ implies that we must have necessarily a negative modulus $\tilde{\mathcal{H}} < 0$ in (3.22), implying the softening response of the material along the discontinuity. ∎

In summary, this analysis shows that the softening response of the material is localized on the discontinuity surface, and characterizes together with the elastic unloading outside this discontinuity the jump observed on Γ. We further assume that the response of the material after bifurcation to the localization mode continues with these characteristics, on a fixed material orientation $\mathbf{N}$ determined by the initial localization condition (3.19) and a localized softening law between $\mathbf{T}_\Gamma$ with $[\![\boldsymbol{\varphi}]\!]$, leading to a stress-displacement relation along Γ. See Section 5.1 for a representative example of these considerations.

4. A New Finite Element Method for Strain Localization.

Previous sections have characterized the different features of strain localization in general multiplicative plasticity models. In particular, the localization mode involving the formation of a strong discontinuity in the deformation $\boldsymbol{\varphi}$ and corresponding singular distributions for the strain measures has been identified. The numerical solution of the problem has then to be able to reproduce these features if a correct simulation of these phenomena is to be expected. In this respect, two important issues need to be resolved correctly:
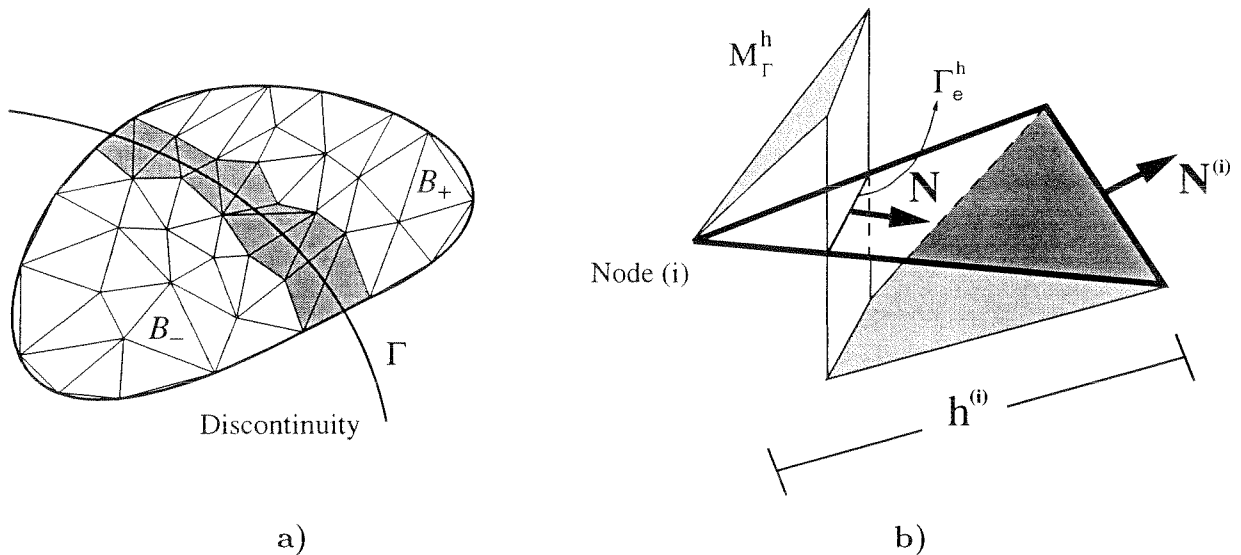
FIGURE 4.1. Finite element interpolations. **a)** Regular triangulation of $\mathcal{B}$. **b)** Discontinuous interpolation function.

1. The localized softening law (3.22) together with the evolution equation for the jump discontinuity (3.26), leading to a localized dissipation along the discontinuity Γ, have to be taken under consideration if a numerical solution independent of the mesh size is to be obtained.

2. Numerical solutions independent of the mesh alignment require an accurate resolution of the *kinematics* of strong discontinuities, as described in Section 3.1. The inclusion of the singular distributions identified in previous sections in the actual finite element interpolations (i.e., solving the limit problem consisting of a strong discontinuity with no smoothing or regularization) appears as a requirement for this purpose.

Standard Galerkin methods do not meet such conditions, thus leading to a overly diffuse resolution of the discontinuities with a strong mesh dependence. The method described below falls within the class of *enhanced strain methods* proposed originally for the infinitesimal range by SIMO & RIFAI [1990], and later extended to the finite strain range by SIMO & ARMERO [1992] and SIMO, ARMERO & TAYLOR [1993]. The essence of the proposed technique is a local enhancement of the finite element interpolations that includes explicitly the localization mode identified in the previous analysis. We present in this section a brief description of the finite element methods that we are currently developing following these ideas.

4.1. A class of enhanced strain methods for localization.

Consider a regular finite element triangulation $\mathcal{B}^h = \cup_{e=1}^{nel} \mathcal{B}_e$ of the reference configuration $\mathcal{B} \approx \mathcal{B}^h$, as depicted in Figure 4.1.a. Let $\varphi^h \in \mathcal{V}^h$ be a finite element interpolation of the deformation $\varphi = \varphi(X)$ satisfying the essential boundary conditions on $\partial_u \mathcal{B}^h$. Denote by $\mathcal{V}_o^h$ the associated test functions, defined explicitly by

$$\mathcal{V}_o^h = \left\{ \boldsymbol{\eta}^h \in [C^0(\mathcal{B}^h)]^{n_{\dim}} \; : \; \boldsymbol{\eta}|_{\mathcal{B}_e^h} \in [P^k(\mathcal{B}_e^h)]^{n_{\dim}} \quad \text{and} \quad \boldsymbol{\eta}^h|_{\partial_u \mathcal{B}^h} = 0 \right\} \tag{4.1}$$

for the space of complete polynomials $P^k(\mathcal{B}_e^h)$ of order $\leq k$. For concreteness, we shall consider in this presentation the simple setting defined by the above Galerkin interpolations based on triangular elements for $n_{\dim} = 2$. The method proposed herein extends easily to general cases involving quadrilateral elements, and general mixed finite elements based on separate interpolation of the deformation and, for instance, the pressure fields. In fact, the numerical simulations presented in Section 5 take as base element for the formulation of the enhanced elements the mixed quadratic triangle $P2$ bubble $/P1$ of CROUZEIX & RAVIART [1973] depicted in Figure 5.1.a.

Standard finite element formulations of the type (4.1) result in a continuous interpolation of the deformation φ. Therefore, they do not possess the localization mode identified in the analysis presented in Section 3. The key idea of the newly proposed finite element methods is to introduce this mode by a local enhancement of the deformation gradient, following (3.3), as

$$\boldsymbol{F}_e^h = \underbrace{\text{GRAD}[\varphi^h]}_{conforming} + \underbrace{\tilde{\boldsymbol{F}}_e^h}_{enhanced} \; . \tag{4.2}$$

After the developments of Section 3.1, we define the *enhanced deformation gradient* $\tilde{\boldsymbol{F}}_e^h$ as

$$\boxed{\tilde{\boldsymbol{F}}_e^h|_{\mathcal{B}_{e,loc}^h} = -\frac{1}{h^{(i)}} (\boldsymbol{\alpha}_e \otimes \boldsymbol{N}^{(i)}) + (\boldsymbol{\alpha}_e \otimes \boldsymbol{N}) \; \delta_\Gamma} \tag{4.3}$$

at the elements $\mathcal{B}_{e,loc}^h$ where localization has been detected with the localization condition (3.19) for a normal $\boldsymbol{N}$. In (4.3), $\boldsymbol{N}^{(i)}$ denotes the normal to the side opposite to node (i) sustaining the discontinuity Γ, and $h^{(i)}$ is the corresponding altitude, as depicted in Figure 4.1.b. The enhanced deformation gradient (4.3) implies a piecewise constant approximation, discontinuous across elements of the localization mode (3.3), with the local element parameters $\boldsymbol{\alpha}_e \in \mathbb{R}^{n_{\dim}}$ approximating the spatial jump $[\![\varphi]\!]$.

Remarks 4.1.

1. The motivation behind (4.3) can be found in the local decomposition (3.1), with the discontinuous part expressed in terms of the discontinuous function

$$M_\Gamma(\boldsymbol{X}) = H_\Gamma(\boldsymbol{X}) - \psi^h(\boldsymbol{X}) \quad \text{in the neighborhood} \quad \Omega_\Gamma \subset \mathcal{B} \; , \tag{4.4}$$

instead of the Heaviside function $H_\Gamma(\boldsymbol{X})$ alone, for some continuous function ψ^h such that $M_\Gamma|_{\partial \Omega^h} = 0$. A finite element approximation of M_Γ is obtained as

$$M_\Gamma^h(\boldsymbol{X}) := H_\Gamma(\boldsymbol{X}) - N^{(i)}(\boldsymbol{X}) \qquad \text{in} \quad \mathcal{B}_{e,loc}^h , \tag{4.5}$$

where $N^{(i)}$ is the linear shape function

$$N^{(i)} = 1 - \frac{(\boldsymbol{X} - \boldsymbol{X}^{(i)}) \cdot \boldsymbol{N}^{(i)}}{h^{(i)}} , \tag{4.6}$$

for node (i) with reference coordinates $\boldsymbol{X}^{(i)}$. The function $M_\Gamma^h(\boldsymbol{X})$ is depicted in Figure 4.1.b. Noting that $\text{GRAD}[N^{(i)}] = -\boldsymbol{N}^{(i)}/h^{(i)}$, a simple calculation shows that $\tilde{\boldsymbol{F}}_e^h = \text{GRAD}[M_\Gamma^h]$.

2. It is important to emphasize that the construction behind (4.5) is not to be understood as defining an incompatible mode field in $\mathcal{B}^h$. Instead, the proposed method falls within the class of assumed enhanced strain methods with the introduction of the enhanced deformation gradient (4.3). The goal is not to construct a discontinuous approximation of the discontinuous deformation φ in (3.1) following, in particular, the different surfaces that appear in this case, but rather to enhance the strain field of the element to capture accurately the localization mode involving singular distributions, as identified in Section 3.2. In particular, the form of the enhanced deformation gradient in (4.3) motivated by the renormalization (4.4) will be exploited in the following section for the construction of the enhanced strain variations satisfying the patch test. ∎

4.2. The enhanced strain variations.

The introduction of the local enhanced parameters $\boldsymbol{\alpha}_e$ requires the addition of a new set of equations to the original weak equilibrium equations (2.1). Following the ideas originally proposed in SIMO & ARMERO [1993], the finite element method proposed herein is based on the weak equations

$$\left. \begin{aligned} \int_\mathcal{B} \boldsymbol{P} : \text{GRAD}[\boldsymbol{\eta}] \, d\mathcal{B} &= \int_\mathcal{B} \boldsymbol{f} \cdot \boldsymbol{\eta} \, d\mathcal{B} + \int_{\partial_t \mathcal{B}} \hat{\boldsymbol{T}} \cdot \boldsymbol{\eta} \, d\Gamma \qquad \forall \boldsymbol{\eta} \in \mathcal{V}_o^h , \\ \int_{\mathcal{B}_{e,loc}} \boldsymbol{P} : \tilde{\boldsymbol{H}}_e^h \, d\mathcal{B} &= 0 \qquad \forall \tilde{\boldsymbol{H}}_e^h \in \tilde{\mathcal{H}}_e^h \quad \text{and} \quad e = 1,2,\dots \text{ (localized elements)} , \end{aligned} \right\} \tag{4.7}$$

for enhanced variations $\tilde{\boldsymbol{H}}_e^h \in \tilde{\mathcal{H}}_e^h$. Equation $(4.7)_1$ corresponds to the usual weak statement of the balance of momentum, imposing weakly the equilibrium of tractions across stress discontinuities (element boundaries) in particular. On the other hand, the test functions $\tilde{\boldsymbol{H}}_e^h$ are designed such that $(4.7)_2$ imposes weakly the compatibility condition (2.5) across the discontinuity Γ. To this end, and motivated by (4.3), we set

$$\tilde{\boldsymbol{H}}_e^h = -\frac{l_S^e}{A_e} (\boldsymbol{\beta}_e \otimes \boldsymbol{N}) + (\boldsymbol{\beta}_e \otimes \boldsymbol{N}) \, \delta_\Gamma \qquad \boldsymbol{\beta}_e \in \mathbb{R}^2 , \tag{4.8}$$

where A_e is the reference area of the element $\mathcal{B}^h_{e,loc}$, and l^e_Γ is the weight assigned to the integration of the delta function δ_Γ, that is

$$\int_{\mathcal{B}^h_{e,loc}} \delta_\Gamma \; d\mathcal{B} = \int_{\Gamma^h_e} d\Gamma = l^e_\Gamma \; , \tag{4.9}$$

where $\Gamma^h_e = \Gamma \cup \mathcal{B}^h_{e,loc}$. One can think of l^e_Γ as the length of the discontinuity line in the element, but as noted in Remark 4.2.1 below the final formulation is independent of the parameter l^e_Γ.

The enhanced strain variations (4.8), satisfy the consistency condition set forth in SIMO & ARMERO [1993]. Namely, constant nominal stress fields are in the solution space (patch test), since in this case (4.7)$_2$ is satisfied identically as

$$\int_{\mathcal{B}^h_{e,loc}} \tilde{\boldsymbol{H}}^h_e \; d\mathcal{B} = (\boldsymbol{\beta}_e \otimes \boldsymbol{N})^s \; [-\frac{l^e_\mathcal{S}}{A_e} \; A_e + l^e_\mathcal{S} \;] = 0 \qquad \forall \boldsymbol{\beta}_e \in \mathbb{R}^2 \; , \tag{4.10}$$

for all localized elements $\mathcal{B}^h_{e,loc}$. Furthermore, the spaces $\tilde{\mathcal{H}}^h_e$ generated by (4.8) and GRAD$[\mathcal{V}^h_o]$ have null intersection, as required in the aforementioned reference.

Inserting (4.8) in (4.7)$_2$, it follows that this last equation imposes

$$\frac{1}{l^e_\Gamma} \int_{\Gamma^h_e} \boldsymbol{T}_\Gamma = \frac{1}{A_e} \int_{\mathcal{B}^h_{e,loc}} \boldsymbol{PN} \; d\mathcal{B} \; , \tag{4.11}$$

where $\boldsymbol{T}_\Gamma = \boldsymbol{PN}|_{\Gamma^h_e}$. For the case of a linear triangle, involving constant stresses $\boldsymbol{P}$ at the element level, this expression reduces to

$$\boldsymbol{T}_\Gamma = \frac{1}{A_e} \int_{\mathcal{B}^h_{e,loc}} \boldsymbol{PN} \; d\mathcal{B} \; . \tag{4.12}$$

Here, the nominal driving traction $\boldsymbol{T}_\Gamma$ is obtained explicitly from the localized softening law along Γ in terms of the jump $\boldsymbol{\alpha}_e$, and the regular stress field $\boldsymbol{P}$ is given by the continuum constitutive law in $\mathcal{B}^h_{e,loc} \backslash \Gamma^h_e$. For higher order triangles, $\boldsymbol{T}_\Gamma$ is approximated similarly by a constant field at each element, as conjugate variable to the jump $\boldsymbol{\alpha}_e$, recovering in this fashion (4.12). One can thing of performing the integration in the left-hand-side of (4.11) by a single quadrature point with weight l^e_Γ. See Remark 4.2.1 and Remark 4.3.1 in this respect.

Remarks 4.2.

1. We note that the basis for the interpolation of the enhanced part of the deformation gradient (4.3), and the enhanced variations (4.8) differ unless $(l^e_\mathcal{S}/A_e)\boldsymbol{N} = (1/h^{(i)})\boldsymbol{N}^{(i)}$. This situation corresponds to the case when Γ^h_e is aligned with one

side of the triangle. This leads to a non-symmetric tangent matrix in the localized elements. This non-symmetry could have been avoided by choosing the same type of interpolation (4.8) in (4.3). However, the formulation presented herein has shown a sharper resolution in capturing strong discontinuities, at the price of symmetry for non-aligned meshes.

2. Equation (4.12) and, therefore, the whole formulation is independent of the particular value of the parameter l_Γ^e. This parameter introduces simply a scaling of the weak equation $(4.7)_2$. The choice $l_\Gamma^e = (\boldsymbol{N} \cdot \boldsymbol{N}^{(i)}) A_e / h^{(i)}$ is preferred, since then symmetry of the linearized equations is recovered in the aligned case, as discussed above. ∎

4.3. Some remarks on the numerical implementation.

An important characteristic of the finite element method outlined in the previous sections is that the delta functions appearing in (4.3) and (4.8) are not smoothed out by an especial regularization technique, as originally presented in SIMO, OLIVER & ARMERO [1993]. Instead, these singular distributions are integrated explicitly leading to the nonlinear finite element equations

$$
\left.
\begin{aligned}
\boldsymbol{R} &:= \boldsymbol{f}^{ext} - \overset{n_{el}}{\underset{e=1}{\mathbf{A}}} \int_{\mathcal{B}_e^h} \boldsymbol{b}_e^T \boldsymbol{\tau} d\mathcal{B} = 0 \ , \\
\boldsymbol{r}_e &:= - \int_{\mathcal{B}_{e,loc}^h} \boldsymbol{g}_e^T \boldsymbol{\tau} \ d\mathcal{B} - \int_{\Gamma_e^h} \boldsymbol{T}_\Gamma \ d\Gamma = 0 \ .
\end{aligned}
\right\}
\tag{4.13}
$$

Clearly, the consequence of maintaining explicitly δ_Γ in (4.8) is translated in the integral along Γ_e^h. As indicated in (4.13), the final implementation is carried out in the current configuration $\varphi^h(\mathcal{B}^h)$, where the sparsity of the matrices involved is recovered (see e.g. SIMO & ARMERO [1993]). In this way, $\boldsymbol{b}_e$ in (4.13) denotes the standard (sparse) strain operator associated to the interpolation of the conforming part in $\mathcal{V}_o^h$, whereas $\boldsymbol{g}_e$ is defined from the regular part of (4.8) as $\boldsymbol{g}_e = -(l_S^e/A_e) \ \boldsymbol{n}$.

Linearization of (4.13) is performed explicitly, carrying material and geometric terms (details are omitted), leading to a numerical implementation that requires only simple modification of existing finite elements. Namely, equation $(4.13)_2$ has to be formed and solved locally at the elements where localization has appeared. An important feature of the proposed approach is that no extra numerical parameters, like a characteristic length common in numerical analyses of the problem at hand, are required. The correct mesh-size independence of the solution is accomplished by the explicit consideration of the localized softening law (3.22) along the strong discontinuity Γ. Similarly, numerical simulations has shown the insensitivity of the proposed methodology to the mesh alignment, as the example in Section 5 illustrates.

Remarks 4.3.

1. As described in Section 4.2, the line integrals along Γ_e^h are computed simply as $\int_{\Gamma_e^h} (\cdot)\, d\Gamma = (\cdot)\, l_\Gamma^e$, since the integrands are approximated by constant fields at the element level. Furthermore, the area integrals in (4.13) do not require a special quadrature rule as it is the case when a band of finite width is present in the element.

2. The extra enhanced modes α_e are only added and solved for when the inception of localization is detected with condition (3.19) at any quadrature point of the element. The element has the option of exciting the two modes corresponding to the two different normals solution of this equation. Adjacent elements pass the information required to determine the correct orientation of the normal, so only one mode is excited in a regular propagation of the slip-line. Alternative procedures for this purpose will be addressed in detail in a future publication.

3. The efficient implementation of the proposed method involves the elimination at the element level of the scalar parameter α_e through a *static condensation*. See SIMO & ARMERO [1993] for further details.   ■

5. A Representative Model Problem.

This section considers the representative model example of plane strain J_2–flow theory. The results obtained in Section 3 are particularized for this case in Section 5.1. Section 5.2 includes representative numerical simulations involving this model problem that demonstrate the independence of the proposed finite element method of the size and the alignment of the mesh.

5.1. Strong discontinuities in plane strain J_2-flow theory.

The case of interest, plane strain J_2-flow theory, is recovered from the equations presented in Section 2.2 by setting $\hat{\omega} \equiv 0$ (i.e. no plastic spin) and

$$\hat{\phi}(\tau) = \sqrt{\frac{3}{2}}\, \| \mathrm{dev}[\tau] \| , \tag{5.1}$$

where $\|s\|^2 = s_{ij}s_{ij}$. The elastic model assumed in the simulation of Section 5.2 corresponds to a regularized logarithmic elastic law (regularized Hencky's law), defined by the stored energy function

$$W(\lambda_1^e, \lambda_2^e) = \tfrac{1}{2}\kappa \left(\log J^e\right)^2 + \mu \left[\left(\log \bar{\lambda}_1^e\right)^2 + \left(\log \bar{\lambda}_2^e\right)^2 \right] \tag{5.2}$$

where $\{\lambda_1^e, \lambda_2^e\}$ denote the elastic principal stretches (square roots of the eigenvalues of C^e) for this plane strain case, and $\bar{\lambda}_A^e = J^{e-1/3} \lambda_A^e$ for $A = 1, 2$. Note that the yield surface (5.1) implies the usual isochoric character of the plastic flow, since

$$n_\phi = \partial_\tau \hat{\phi} = \sqrt{\frac{3}{2}} \frac{\text{dev}[\tau]}{\|\text{dev}[\tau]\|} \qquad \Rightarrow \qquad \text{tr}[n_\phi] = 0 \ , \tag{5.3}$$

leading to $J^p = \det F^p = 1$ and, consequently, $J = J^e = \lambda_1^e \lambda_2^e$. In (5.2), κ and μ denote the bulk and shear modulus, respectively.

The results presented in Section 3.1 apply directly to this case, in particular, the localization condition (3.19) involving the perfectly plastic tangent. A particularly simple expression of this condition is obtained by noting the different order of magnitude of the yield limit σ_y (and, consequently, the stresses τ) and the elastic moduli in metals ($\sigma_y/\mu \approx 10^{-3}$). Neglecting then small geometric terms of order $o(\sigma_y/\mu)$, we conclude as a first approximation

$$0 = Q_{ep} \pmb{\mathcal{L}}_v[\![\varphi]\!] \approx \left\{ n \cdot \left[\mathbf{a}_e - \frac{1}{n_\phi : \mathbf{a}_e n_\phi} \mathbf{a}_e n_\phi \otimes \mathbf{a}_e n_\phi \right] n \right\} \pmb{\mathcal{L}}_v[\![\varphi]\!]$$

$$\implies \qquad \text{sym}\,[\pmb{\mathcal{L}}_v[\![\varphi]\!] \otimes n] \propto n_\phi \tag{5.4}$$

The approximation in (5.4) is classical for the problem at hand. Details can be found in ASARO [1983], together with complete evaluations of the localization condition (3.19) without the involvement of the above approximation. The reduced localization condition $(5.4)_2$ will suffice for our purposes. In this case, $(5.4)_2$ coincides with its counterpart in the infinitesimal case (ARMERO & GARIKIPATI [1995]). From (5.3) we conclude

$$\text{tr}[n_\phi] = 0 \qquad \Rightarrow \qquad \pmb{\mathcal{L}}_v[\![\varphi]\!] \cdot n = 0 \tag{5.5}$$

recovering then the classical concept of a slip-line. Moreover, condition $(5.4)_2$ implies that the slip-line direction N bisects the principal stress directions in a first approximation; see ARMERO & GARIKIPATI [1995] for details.

Similarly, the expression for the evolution of the jump (3.26) in the localization mode can be simplified as follows. Consider the orthonormal basis $\{M, N\}$ in the reference configuration $\mathcal{B}$, with N being the unit normal determined by the localization condition. Consider the convected basis $\{m^\sharp, n^\sharp\}$ in the current configuration $\varphi(\mathcal{B})$ defined by

$$m^\sharp = \bar{F} M \qquad \text{and} \qquad n^\sharp = \bar{F} N \ , \tag{5.6}$$

where $\bar{F}$ is the regular part of the deformation gradient as introduced in Section 3. The vector $m^\sharp$ is not a unit vector necessarily, but it satisfies $m^\sharp \cdot n = M \cdot N = 0$. A particularly convenient expression of the jump $[\![\varphi]\!]$ is obtained in the convected basis (5.6) as

$$[\![\varphi]\!] = \xi_n n^\sharp + \xi_m m^\sharp \qquad \Longleftrightarrow \qquad J = \bar{F}^{-1}[\![\varphi]\!] = \xi_n N + \xi_m M \ , \tag{5.7}$$

with normal ξ_n and tangential ξ_m components. The use of the relation $(3.9)_3$ leads to the explicit expression

$$\boldsymbol{\mathcal{L}}_v[\![\varphi]\!] = \dot{\xi}_n \boldsymbol{n}^\sharp + \dot{\xi}_m \boldsymbol{m}^\sharp \tag{5.8}$$

for the Lie derivative of the jump. Relation (5.5) implies $\dot{\xi}_n = 0$, and $\xi_m \geq 0$ by (3.24) and (3.26), implying the irreversibility of the localized flow (the vector $\boldsymbol{M}$ is assumed in the direction of the slip). Equation (3.26) implies then

$$\dot{\xi}_m = \frac{1}{\Xi \bar{H}} \boldsymbol{n}_\phi : \left.\overset{\triangledown}{\tau}\right|_\Gamma \qquad \text{where} \qquad \Xi := \frac{\mathbf{a}_e \boldsymbol{n}_\phi : \left(\boldsymbol{n} \otimes \boldsymbol{m}^\sharp\right)^s}{\boldsymbol{n}_\phi : \mathbf{a}_e \boldsymbol{n}_\phi} . \tag{5.9}$$

Define the *resolved shear stress* (the "Schmid stress") as

$$T_m := \boldsymbol{m}^\sharp \cdot \boldsymbol{\tau} \boldsymbol{n} = \boldsymbol{m}^\sharp \cdot \boldsymbol{T}_\Gamma . \tag{5.10}$$

A calculation using relations (5.6) and (5.10) results in

$$\dot{T}_m = \boldsymbol{m}^\sharp \cdot [\overset{\triangledown}{\tau} + \bar{\boldsymbol{d}}\boldsymbol{\tau} - \boldsymbol{\tau}\bar{\boldsymbol{d}}]\boldsymbol{n} , \tag{5.11}$$

see ASARO [1983]. Neglecting small geometric terms of order $o(\sigma_y/\mu)$, relation (5.9) implies as a first approximation the softening law

$$\boxed{\dot{T}_m = \hat{H}(\xi_m)\dot{\xi}_m , \qquad \text{with} \quad \dot{\xi}_m \geq 0 ,} \tag{5.12}$$

for some general softening modulus $\hat{H} = \hat{H}(\xi_m)$. The law relates the rates of resolved shear stress $\dot{T}_m$ with the rate of slip $\dot{\xi}_m$, and is, therefore, an objective relation. As noted in Section 3, after localization the material direction $\boldsymbol{N}$ is assumed fixed, with the softening law assumed along the discontinuity. The classical *Schmid law* is, therefore, effectively recovered in this case. The reader is referred to the comprehensive review article by ASARO [1983] for further details.

Remark 5.1. The finite element method described in Section 4 approximates the jump $[\![\varphi]\!]$ by $\boldsymbol{\alpha}_e \in \mathbb{R}^2$ at the element level. In the present case, however, the normal component of the jump vanishes by (5.5). In the numerical simulations presented in the following section, this constraint is regularized by penalization as

$$T_n := \boldsymbol{n} \cdot \boldsymbol{T}_\Gamma = k_n \, \xi_n . \tag{5.13}$$

where $\xi_n = \boldsymbol{n} \cdot \boldsymbol{\alpha}_e$, and penalty parameter k_n. In the limit as $k_n \to \infty$, the constraint (5.5) is recovered, while maintaining the structure described in the Section 4 for the finite element method. Formulations imposing (5.5) exactly can be easily devised. The finite element equations are then completely defined with the nominal driving traction defined as

$$\boldsymbol{T}_\Gamma = T_n \boldsymbol{n} + T_m \boldsymbol{m}^\flat , \qquad \text{where} \quad \boldsymbol{m}^\flat = \bar{\boldsymbol{F}}^{-T} \boldsymbol{M} , \tag{5.14}$$
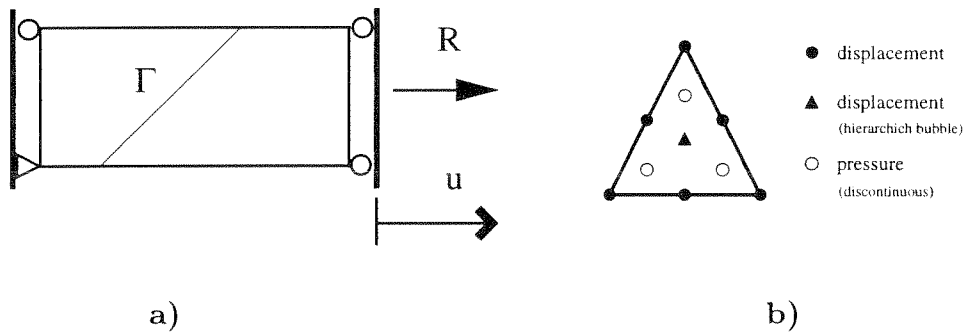
FIGURE 5.1. Tension test. **a)** Problem definition (8×3 computational domain). **b)** Base element: $P2 \oplus \text{bubble}/P1$, with (7 node) quadratic displacements and discontinuous linear pressure.

with T_n and T_m given by (5.13) and (5.10), respectively, in terms of the slip $\xi_m = \boldsymbol{m}^b \cdot \boldsymbol{\alpha}_e$ and (regularized) normal jump $\xi_n = \boldsymbol{n} \cdot \boldsymbol{\alpha}_e$.   ∎

5.2. Representative numerical simulations.

This section presents a number of representative numerical simulations based on the new finite element methods proposed herein. The goals are twofold: to show the independence of these methods on 1) the mesh size, and 2) the mesh alignment. For this purpose, the simple setting given by the model problem of plane strain J_2–flow theory described in Section 5.1 is considered. In particular, the regularized logarithmic hyperelastic law (5.2) is assumed with $\kappa = 164.206$ and $\mu = 80.1938$. The yield limit is $\sigma_y = 0.45$, with a *(localized) linear softening law* (3.22) with softening modulus $\bar{H} = -5$. As described in the previous sections, the softening is introduced with the localization condition is satisfied for some $\boldsymbol{N}$. In this case, this condition reduces to (5.4)$_2$ which can be expressed in closed-form (see ARMERO & GARIKIPATI [1995]), with the slip-lines bisecting the principal directions.

We consider the plane strain tension test as a benchmark problem; see TVERGAARD & NEEDLEMAN [1984] and references therein for other numerical studies of this problem. The problem definition is depicted Figure 5.1.a. A small material imperfection is introduced to trigger the localization of the flow in these perfectly symmetric situation; the yield limit is reduced by 1% in one element at the lower boundary. The mixed triangle $P2 \oplus \text{bubble}/P1$, consisting of quadratic interpolations of the displacement field with a hierarchic bubble (7 node triangle), and linear discontinuous pressure interpolation, is considered as the base element to which the enhanced modes described in Section 4 are added. This element, depicted in Figure 5.1.b, was originally proposed in CROUZEIX & RAVIART [1973] and satisfies the LBB condition. The motivation for the consideration of this type of elements is the need to avoid the locking response of standard isoparametric elements
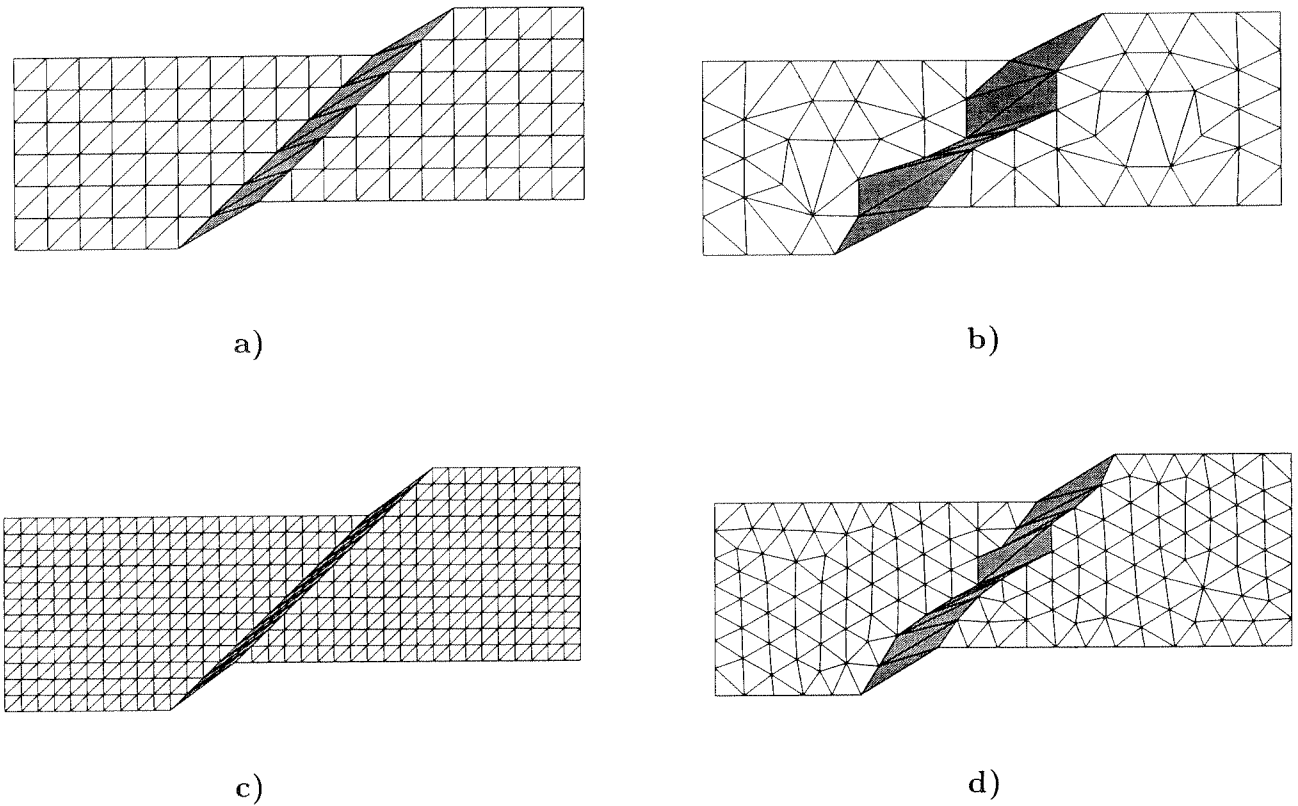
a)

b)

c)

d)

FIGURE 5.2. Tension test. Deformed configurations at an imposed displacement of 0.75 computed with the $P2 \oplus$ bubble$/P1$ triangle with enhanced modes: **a)** Structured mesh, 192 elements; **b)** Structured mesh, 768 elements; **c)** Unstructured mesh, 100 elements; **d)** Unstructured mesh, 254 elements. The elements with excited enhanced localization modes are shown in gray.

due to the isochoric plastic response present in the problem before localization.

Figure 5.2 shows the solutions obtained by the proposed enhanced finite elements. Structured and unstructured meshes are considered, involving from 100 to 768 elements. The deformed configurations shown in this figure demonstrate the ability of the elements to simulate the localization mode with a complete general mesh unrelated to the final solution. The elements shown in gray scale have excited enhanced modes. More importantly, the load-displacement curves are included for the different simulations in Figure 5.3 showing the independence of the present methods on the mesh size and alignment. The curves for the four different meshes literally overlap.

Standard Galerkin methods not only show the well-known strong dependence on the mesh size, but also strong dependence on mesh alignment. Good resolution can be
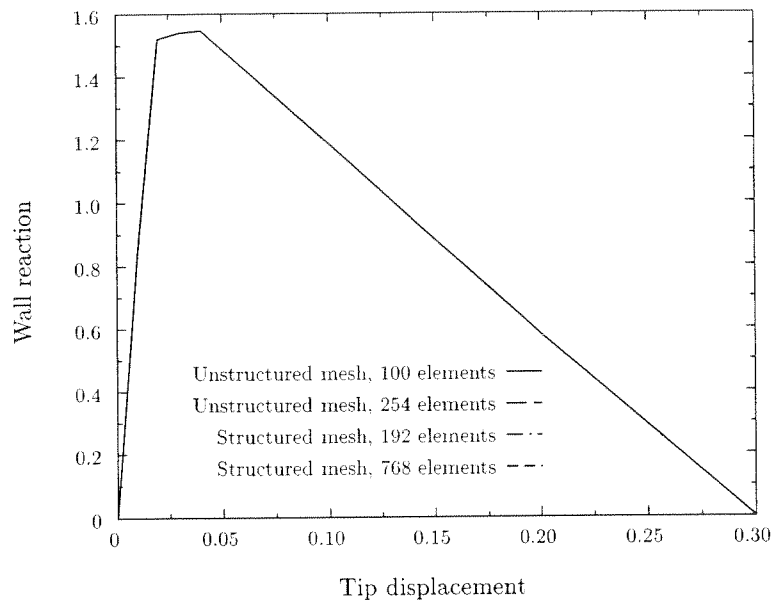
FIGURE 5.3. Tension test. Load-displacement curves for the different solutions shown in Figure 5.2. The independence of the solution on the mesh size and mesh alignment is readily apparent.
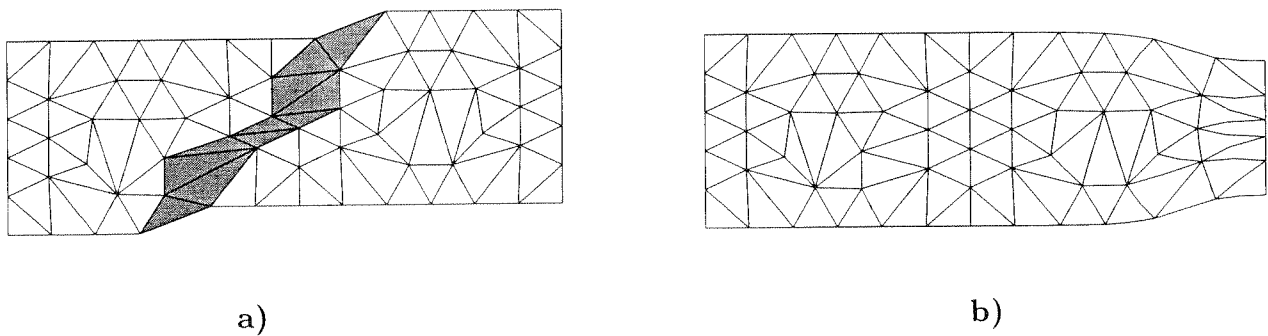

a)   b)

FIGURE 5.4. Tension test. Comparison of the solutions obtained with the $P2 \oplus \text{bubble}/P1$ triangle **a)** with, and **b)** without enhanced localization modes, for an unstructured mesh (100 element) in the perfect plasticity limit ($\bar{H} = 10^{-2}$). Relative slip = 0.45. The overly stiff (and non-objective) response of standard mixed methods is to be contrasted with the enhanced element. The elements with excited enhanced localization modes are shown in gray.

obtained with aligned meshes, but in general they are too stiff when general unstructured meshes are considered. Figure 5.4 shows the solution obtained by the mixed triangle of Figure 5.1.b with and without modes, and a unstructured 100 element mesh. The perfectly plastic limit is effectively recovered by setting $\bar{H} = -10^{-4}$; for the elment without modes, a continuum (non-localized) linear softening law is considered with this modulus. While the enhanced formulation is able to capture the localization of the strains, the standard mixed triangle leads to a solution involving diffuse necking. In both cases, the material imperfection is present, but due to the overly stiff response of the mixed element without the modes the localization mode is lost in this case.

6. Concluding Remarks.

An analysis of strong discontinuities has been presented in the fully nonlinear context of multiplicative finite strain plasticity with strain-softening. This analysis shows that solutions involving this type of discontinuities can be completely characterized by making formal sense of the continuum relations in distributional form. In particular, a distributional softening modulus has been obtained for the localization mode. Physically, the softening response of the material is localized along the discontinuity.

This analysis is a first formal attempt to extend to the finite strain range some well-known results of discontinuous solutions in infinitesimal plasticity. A complete mathematical description of the results and ideas presented herein are currently under investigation. In fact, a complete existence and regularity theory for finite strain plasticity is still lacking and appears to be a very challenging task.

In addition, the introduction of the localization mode identified in the analysis in finite element interpolations through the enhanced strain methodology has led to finite element formulations especially suited for this class of problems. These methods lead to a sharp resolution of strong discontinuities, and have shown not only their independence to the mesh size, but also a strong insensitivity to the mesh alignment. These properties have been accomplished by the introduction of singular distributions (delta functions) in the finite element spaces, without any kind of smoothing or regularization. The final numerical implementation does not require in this manner any numerical ad-hoc (regularization) parameter.

References

ANAND, L. [1985] "Constitutive Equations for Hot Working of Metals", *Int. J. Plasticity,* **1**, 213-231.

ANZELLOTTI, G. & GIAQUINTA, M. [1982], "On the Existence of the Fields of Stresses and Displacements for an Elasto-Perfectly Plastic Body in Static Equilibrium", *J. Math Pures et Appliquées,* **61**, 219-244.

ARMERO, F. & GARIKIPATI, K. [1995] "Recent Advances in the Analysis and Numerical Simulation of Strain Localization in Inelastic Solids," *Proceedings of Computational Plasticity IV,* ed. by D.R.J. Owen, E. Onate, and E. Hinton, CIMNE, Barcelona, Spain, April 1995, 547-561.

ASARO [1983] "Micromechanics of Crystals and Polycrystals", *Advances in Applied Mechanics,* **23**, 1-115.

BALL, J.M., [1977], "Convexity Conditions and Existence Theorems in Nonlinear Elasticity," *Archive for Rational Mechanics and Analysis,* **63**, 337-403.

BAZANT, Z.P.; BELYTSCHKO, M. & CHANG, T.P. [1984] "Continuum Theory for Strain-Softening", *J. Eng. Mech., ASCE,* **110**, 1666-1691.

BELYTXCHKO, T.; FISH, J. & ENGELMANN, B. [1988] "A Finite Element with Embedded Localization Zones", *Comp. Meth. Appl. Mech. Eng.,* **70**, 59-89.

DE BORST, R. & SLUYS, L.J. [1991] "Localization in a Cosserat Continuum under Static and Loading Conditions", *Comp. Meth. Appl. Mech. Eng.,* **90**, 805-827.

CIARLET, P.G. [1988] *Mathematical Elasticity. Volume I: Three Dimensional Elasticity,* North-Holland, Amsterdam.

COLEMAN, B.D. & HODGON, M.L. [1985] "On Shear Bands in Ductile Materials", *Arch. Rat. Mech. Analy.,* **90**, 219-247.

CROUZEIX, M.& RAVIART, P.A. [1973] "Conforming and nonconforming finite element methods for solving the stationary Stokes equations", *R.A.I.R.O. Anl. Numer.,* **7**, 33-76.

DAFALIAS, Y.F. [1984] "A Missing Link in the Formulation and Numerical Implementation of Finite Transformation Plasticity", in *Constitutive Equations: Macro and Computational Aspects,* ed. by K.J. Willam, ASME.

DUVAUT, G. & LIONS, J.L. [1972] *Inequalities in Mechanics and Physics,* Springer Verlag, Berlin.

HADAMARD, J. [1903] *Lecons sur la Propagation des Ondes et les Equations de l' Hydrodynamique,* Chap. IV, Paris, Hermann.

HILL, R. [1950] *The Mathematical Theory of Plasticity*, Oxford University Press

HILL, R. [1962] "Acceleration Waves in Solids", *J. Mech. Phys. Solids*, **16**, 1-10.

HILLERBORG, A. [1985] "Numerical Methods to Simulate Softening and Fracture of Concrete", in *Facture Mechanics of Concrete: Structural Application and Numerical Calculation*, ed. by G.C. Sih and DiTomasso, 141-170.

JOHNSON, C. [1976] "Existence Theorems for Plasticity Problems", *J. Math. Pures et Appliquées*, **55**, 431-444.

JOHNSON, W. [1987] "Henri Tresca as the Originator of Adiabatic Heat Lines", *Int. J. Mech. Science*, **29**, 301-310.

KACHANOV, L.M. [1971] *Foundations of the Theory of Plasticity*, North-Holland.

MANDEL, J. [1966] "Conditions de Stabilité et Postulat de Drucker", in *Rheology and Soli Mechanics*, IUTAM Symposium, Grenoble 1964, ed. by J. Kravtchenko and P.M. Sirieys, 58-68.

MATTHIES, H.; STRANG, G. & CHRISTIANSEN, E. [1979] "The Saddle Point of a Differential Program", in *Energy Methods in Finite Element Analysis*, ed. by Glowinski, Rodin & Zienkiewicz, J. Wiley & Sons.

MOHAN, B., ORTIZ, M. & SHIH, C.F. [1990], "Formulation of Implicit Finite Element Methods for Multiplicative Deformation Plasticity", *Int. J. Num. Meth. Eng.*, **29**, 483-514.

NACAR, A.; NEEDLEMAN, A.& ORTIZ, M. [1989] "A finite element method for analyzing localization in rate dependent solids at finite strains", *Comp. Meth. Appl. Mech. Eng.*, **73**, 235-258.

OLIVER, J. [1989] "A Consistent Characteristic Length for Smeared Cracking Problems", *Int. J. Num. Meth. Eng.*, **28**, 461-474.

RICE, J. [1976] "The Localization of Plastic Deformations", in *Theoretical and Applied Mechanics*, ed. by W.T. Koiter, 207-219.

SHAWKI, T.G. & CLIFTON, R.J. [1989] "Shear Band Formation in Thermal Viscoplastic Materials", *Mech. Mat.*, **8**, 13-43.

SIMO [1995] "Numerical Analysis of Classical Plasticity", *Handbook for Numerical Analysis, Volume IV*, ed. by P.G. Ciarlet and J.J. Lions, in press.

SIMO, J.C. & ARMERO, F. [1992] "Geometrically Non-Linear Enhanced Strain Mixed Methods and the Method of Incompatible Modes", *Int. J. Num. Meth. Eng.*, **33**, 1413-1449.

SIMO, J.C.; ARMERO, F. & TAYLOR, R.L. [1994] "Improved Versions of Assumed

Enhanced Strain Tri-Linear Elements for 3D Finite Deformation Problems", *Comp. Meth. App. Mech. Engin.*, **110**, 359.

SIMO, J.C.; OLIVER, J. & ARMERO, F. [1993] "An Analysis of Strong Discontinuities Induced by Softening Solutions in Rate-Independent Solids", *J. Comput. Mech.*, **12**, 277-296.

SIMO, J.C. & OLIVER, J. [1994] "A New Approach to the Analysis and Simulation of Strain-Softening in Solids", *Fracture and Damage in Quasi-Brittle Materials*, ed. by Bazant et al., Prague.

SIMO, J.C. & RIFAI, M.S. [1990] "A Class of Mixed Assumed Strain Methods and the Method of Incompatible Modes", *Int. J. Numer. Meth. Eng.*, **29**, 1595-1638.

SUQUET, P.M. [1981] "Sur les Equations de la Plasticité: Existence et Regularité des Solutions", *J. Mech.*, **20**, 5-39.

SUQUET, P.M. [1978] "Existence and regularity of Solutions for Plasticity Problems", in *Variational Methods in Mechanics of Solids*, ed. by Nemat-Nasser, 304-309.

TEMAM, R. [1986] "A Generalized Norton-Hoff Model and the Prandtl-Reuss Law of Plasticity", *Arch. Rat. Mech. Anal.*, **95**, 137-183.

TEMAM, R. & STRANG, G. [1980] "Functions of Bounded Deformation", *Arch. Rat. Mech. Anal.*, **75**, 7-21.

THOMAS, T.Y. [1961] *Plastic Flow and Fracture in Solids*, Academic Press.

TRUESDELL C. & W. NOLL, [1965], *The nonlinear field theories*, Handbuch der Physik, Band III/3, Springer, Berlin.

TVERGAARD, V. & NEEDLEMAN, A. [1984] "Finite Element Analysis of Localization Plasticity", in *Finite Elements, Volume V*, ed. by J.T. Oden and G.F. Carey, Prentice Hall, Englewood Cliffs.

ZIENKIEWICZ, O.C. [1992] "Computational Mechanics Today", *Int. J. Num. Meth. Eng.*, **34**, 9-33.